CHEMISTRY OF MATERIALS
Article

Chem. Mater. **2009,** *21,* 5099–5111 5099
DOI:10.1021/cm901901j

Ligand-Assisted Rational Design and Supramolecular Tectonics toward Highly Luminescent Eu^{3+}-Containing Organic−Inorganic Hybrids

Patrícia P. Lima,[†] Filipe A. Almeida Paz,[‡] Rute A. S. Ferreira,[†] V. de Zea Bermudez,[§] and Luís D. Carlos*,[†]

[†]*Departamento de Física and* [‡]*Departamento de Química, Universidade de Aveiro CICECO, 3810-193 Aveiro, Portugal, and* [§]*Departamento de Química and CQ-VR, Universidade de Trás-os Montes e Alto Douro, 5001-801 Vila Real, Portugal*

Received June 30, 2009. Revised Manuscript Received September 4, 2009

The ligands−assisted rational design of a Eu^{3+}-containing organic−inorganic hybrid (di-ureasil) displaying the highest emission quantum yield (0.60 ± 0.06) reported so far is introduced. Two new lanthanide complexes were synthesized in which the metal (Eu^{3+} or Gd^{3+}) first coordination sphere is formed by three β-diketonate ligands (btfa is the 4,4,4-trifluoro-l-phenyl-1,3-butanedionate ion) and two methanol (MeOH) molecules. The complexes also comprise the bpeta (1,2−bis(4−pyridyl)ethane) ligand. The Eu^{3+} complex crystal structure, determined by single crystal X−ray diffraction, confirms the hydrogen bonding ability, the high conformational flexibility and the versatile binding mode of the N, N′-bidentate bpeta in the architecture of the crystals. The bpeta spacers act as bridges, promoting the formation of supramolecular dimeric $[Eu(btfa)_3(MeOH)_2]_2bpeta_2$ species via the establishment of highly directional and strong hydrogen−bonds between the bpeta N atoms and the OH groups of the MeOH molecules. The synthesis of the Eu^{3+}-doped di-ureasils is an efficient three-step concerted process that results in the destruction of the bpeta-driven self-assembled dimeric units and the formation of a new complex in which the di-ureasil structure plays the role of ligand: (i) one or two labile MeOH molecules are released from the ion local environment and replaced by the oxygen atoms of the carbonyl groups of the urea cross-links; (ii) an increase in the degree of order of the poly(oxyethylene) (POE) chains occurs concomitantly; (iii) the bpeta ligand remains in the neighborhood of the newly formed Eu^{3+} complex. The synergy between the absorption ability of the btfa and bpeta cromophores and the hybrid's emitting centers creates additional and efficient bpeta-to-hybrid and bpeta-to-btfa transfer channels that optimize the metal sensitization process contributing for the large measured emission quantum yield.

Introduction

Over the past decade the interest in lanthanide-containing organic−inorganic hybrids has grown considerably with the concomitant fabrication of materials with tunable attributes and offering modulated properties. The potential of these materials relies on the possibility of fully exploiting the synergy between the intrinsic characteristics of sol−gel derived hosts (e.g., highly controlled purity, easy shaping and patterning, easy control of the refractive index, excellent optical quality, photosensitivity, encapsulation of large amounts of emitting centers isolated from each other and protected by the host), and the luminescence features of trivalent lanthanide ions (Ln^{3+}) (e.g., high emission quantum yield, narrow bandwidth and long-lived emission, large Stokes shifts, ligand−dependent luminescence sensitization). Promising applications may be envisaged, such as light-emitting devices, active waveguides in the visible (vis) and near IR (NIR) spectral regions, active coatings, and biomedical actuators and sensors, opening up exciting directions in materials science and related technologies with significant implications in the integration, miniaturization, and multifunctionalization of devices.[1−5]

The research activity in this field has been essentially focused on amorphous organic−inorganic siloxane-based hybrids, either incorporating added lanthanide compounds (ionic salts[6−8] or organic complexes[9−14]) or formed through the covalent attachment bonding

*Corresponding author. Tel: +351-234-370946. Fax: +351-234-378197. E-mail: lcarlos@ua.pt.

(1) Carlos, L. D.; Ferreira, R. A. S.; de Zea Bermudez, V.; Ribeiro, S. J. L. *Adv. Mater.* **2009**, *21*, 509.
(2) Escribano, P.; Julian−Lopez, B.; Planelles−Arago, J.; Cordoncillo, E.; Viana, B.; Sanchez, C. *J. Mater. Chem.* **2008**, *18*, 23.
(3) Carlos, L. D.; Ferreira, R. A. S.; de Z. Bermudez, V. In *Hybrid Materials*; Kickelbick, G., Ed.; Wiley-VCH: Weinheim, Germany, 2007; pp. 337−400.
(4) Sanchez, C.; Julian, B.; Belleville, P.; Popall, M. *J. Mater. Chem.* **2005**, *15*, 3559.
(5) Sanchez, C.; Lebeau, B.; Chaput, F.; Boilot, J. P. *Adv. Mater.* **2003**, *15*, 1969.
(6) Carlos, L. D.; Ferreira, R. A. S.; de Zea Bermudez, V.; Molina, C.; Bueno, L. A.; Ribeiro, S. J. L. *Phys. Rev. B* **1999**, *60*, 10042.
(7) Carlos, L. D.; Messaddeq, Y.; Brito, H. F.; Ferreira, R. A. S.; Bermudez, V. D.; Ribeiro, S. J. L. *Adv. Mater.* **2000**, *12*, 594.
(8) Ferreira, R. A. S.; Carlos, L. D.; Goncalves, R. R.; Ribeiro, S. J. L.; de Zea Bermudez, V. *Chem. Mater.* **2001**, *13*, 2991.
(9) Binnemans, K. In *Handbook on the Physics and Chemistry of Rare Earths*; Gschneidner, Jr., K. A., Bunzli, J. C. G., Pecharsky, V. K., Eds.; Elsevier: Amsterdam, 2005; Vol. *35*, Chapter 225, pp. 107−272.
(10) Lima, P. P.; Ferreira, R. A. S.; Freire, R. O.; Paz, F. A. A.; Fu, L.; Júnior, S. A.; Carlos, L. D.; Malta, O. L. *ChemPhysChem* **2006**, *7*, 735.

Published on Web 10/16/2009

grafting of these complexes to the siliceous skeleton.[15−18] More recently, considerable efforts of the community of hybrid materials have been focused on materials tectonics, in particular in the organization and texturing of Ln^{3+}-doped organic−inorganic hybrids obtained through the combination of sol−gel routes and self-assembly processes in the presence of external structure-directing agents (template-directed assembly[19−22] or in their absence (self-directed assembly[23]).

Among the Ln^{3+}-containing organic−inorganic hybrids reported in the last two decades, the most efficient systems are di-ureasils (a series of hybrid frameworks consisting of a siliceous skeleton grafted to poly(oxyethylene) (POE) chains through urea groups and represented by the notation d-U(Y), where Y stands for the average molecular weight of the polymer chains)[27] doped with Eu^{3+} β-diketonate complexes (Table 3 of ref 1), due to the high UV absorption cross section and efficient energy transfer to the Ln^{3+} centers of the β-diketonate ligands[9] and hybrid's emitting centers.[24−26]

It is worth mentioning the case of the hybrid material formed through embedding of the [Eu(btfa)$_3$(4,4′-bpy)-(EtOH)] (btfa is the 4,4,4-trifluoro-1-phenyl-1,3-butanedionate ion, 4,4′-bpy is 4,4′-bipyridine and EtOH is ethanol) complex into the d-U(600) di-ureasil network for which a maximum quantum yield of 0.51 was found,[10] a value significantly higher than that reported for the isolated complex (0.37). A similar effect was observed in the d-U(2000)-co-d-U(600) co-condensed di-ureasil structure doped with Eu(tta)$_3\cdot 2H_2O$ (tta is the 4,4,4-trifluoro-1-(2-thienyl)-1,3-butanedionate ion), where the quantum yield increased from 0.29 to 0.36 upon complex incorporation.[28] The di-ureasil hybrid host also contributed to the enhancement of the poor quantum yield of the Eu(nta)$_3$bipy (nta is the 4,4,4-trifluoro-1-(2-naphthyl)-1,3-butanedionate ion) complex (from 0.07 to 0.15).[13] All theses examples stress the active and manifold role played by the hybrid host in (1) light harvesting, (2) energy transfer to the Eu^{3+} ions, and (3) lanthanide first coordination sphere composition through replacement of labile ligands (e.g., water or alcohol molecules) by groups with strong coordinating ability provided by the hybrid itself, such as the C=O groups of the urea cross-links.

The innovative concept addressed in the present paper is the use of a ligand-assisted rational synthesis strategy to design highly efficient light-emitting Ln^{3+}-containing organic−inorganic hybrids, which in the case of the Eu^{3+}-containing sample yields the highest emission quantum yield reported so far, 0.60 ± 0.06. The basic principle of this new synthetic approach relies on the suitable design of the isolated complex. Here the Eu^{3+}-first coordination shell encompasses light-harvesting btfa ligands with high absorption cross sections for efficient metal emission sensitization and labile methanol (MeOH) molecules (Figure 1). The complex also comprises the flexible bidentate bpeta (where bpeta is 1,2-bis(4-pyridyl)ethane) active molecular construction unit (tecton) (Figure 2). We note that, although the most widely used acronym for this ligand is bpe,[29] we have decided to adopt here instead the acronym suggested by Roesky and Andruh[30] to avoid any confusion with the 1,2-bis(4-pyridyl)ethene ligand for which the acronym proposed is also bpe.[31] The well-known hydrogen bonding acceptor and bridging ability of bpeta have been employed here to induce the formation of dimeric units of the complex via hydrogen bonds established between the N atoms of the bpeta cromophore and the OH groups of the MeOH molecules (Figure 2). Although not directly coordinated to the Eu^{3+} ion, this cromophore molecule contributes to the overall Eu^{3+} sensitization. After incorporation into the di-ureasil hybrid host, the hydrogen bonds are broken, as the C=O groups of the urea cross-links of the hybrid host structure penetrate the cation first coordination shell, simultaneously expelling the MeOH molecules (Scheme 1). An increase of the degree of order of the POE chains aids this concerted mechanism. Considering the considerable bulkiness of both the bpeta molecule and specially the d-UPTES(600) precursor molecule (see Experimental Section), the whole effect is globally quite impressive from the structural standpoint,

(11) Franville, A. C.; Zambon, D.; Mahiou, R.; Troin, Y. *Chem. Mater.* **2000**, *12*, 428.
(12) Moleski, R.; Stathatos, E.; Bekiari, V.; Lianos, P. *Thin Solid Films* **2002**, *416*, 279.
(13) Fu, L. S.; Ferreira, R. A. S.; Silva, N. J. O.; Fernandes, J. A.; Ribeiro-Claro, P.; Goncalves, I. S.; de Zea Bermudez, V.; Carlos, L. D. *J. Mater. Chem.* **2005**, *15*, 3117.
(14) Lima, P. P.; Junior, S. A.; Malta, O. L.; Carlos, L. D.; Ferreira, R. A. S.; Pavithran, R.; Reddy, M. L. P. *Eur. J. Inorg. Chem.* **2006**, 3923.
(15) Sun, L. N.; Zhang, H. J.; Meng, Q. G.; Liu, F. Y.; Fu, L. S.; Peng, C. Y.; Yu, J. B.; Zheng, G. L.; Wang, S. B. *J. Phys. Chem. B* **2005**, *109*, 6174.
(16) Wang, Q. M.; Yan, B. *Cryst. Growth Des.* **2005**, *5*, 497.
(17) Lenaerts, P.; Storms, A.; Mullens, J.; D'Haen, J.; Gorller-Walrand, C.; Binnemans, K.; Driesen, K. *Chem. Mater.* **2005**, *17*, 5194.
(18) Armelao, L.; Bottaro, G.; Quici, S.; Cavazzini, M.; Raffo, M. C.; Barigelletti, F.; Accorsi, G. *Chem. Commun.* **2007**, 2911.
(19) da Silva, L. C. C.; Martins, T. S.; Filho, M. S.; Teotonio, E. E. S.; Isolani, P. C.; Brito, H. F.; Tabacniks, M. H.; Fantini, M. C. A.; Matos, J. R. *Microporous Mesoporous Mater.* **2006**, *92*, 94.
(20) Gago, S.; Fernandes, J. A.; Rainho, J. P.; Ferreira, R. A. S.; Pillinger, M.; Valente, A. A.; Carlos, T. M.; Santos; Carlos, L. D.; Ribeiro−Claro, P. J. A.; Goncalves, I. S. *Chem. Mater.* **2005**, *17*, 5077.
(21) Guo, X. M.; Fu, L. S.; Zhang, H. J.; Carlos, L. D.; Peng, C. Y.; Guo, J. F.; Yu, J. B.; Deng, R. P.; Sun, L. N. *New J. Chem.* **2005**, *29*, 1351.
(22) Meng, Q. G.; Boutinaud, P.; Zhang, H. J.; Mahiou, R. *J. Lumin.* **2007**, *124*, 15.
(23) Nobre, S. S.; Brites, C. D. S.; Ferreira, R. A. S.; de Zea Bermudez, V.; Carcel, C.; Moreau, J. J. E.; Rocha, J.; Man, M. W. C.; Carlos, L. D. *J. Mater. Chem.* **2008**, *18*, 4172.
(24) Carlos, L. D.; Ferreira, R. A. S.; de Zea Bermudez, V.; Ribeiro, S. J. L. *Adv. Funct. Mater.* **2001**, *11*, 111.
(25) Carlos, L. D.; Ferreira, R. A. S.; Pereira, R. N.; Assunção, M.; de Zea Bermudez, V. *J. Phys. Chem. B* **2004**, *108*, 14924.
(26) Nobre, S. S.; Lima, P. P.; Mafra, L.; Ferreira, R. A. S.; Freire, R. O.; Fu, L.; Pischel, U.; de Zea Bermudez, V.; Malta, O. L.; Carlos, L. D. *J. Phys. Chem. C* **2007**, *111*, 3275.
(27) de Zea Bermudez, V.; Carlos, L. D.; Alcácer, L. *Chem. Mater.* **1999**, *11*, 569.
(28) Fernandes, M.; de Zea Bermudez, V.; Ferreira, R. A. S.; Carlos, L. D.; Martins, N. V. *J. Lumin.* **2008**, *128*, 205.
(29) Fujita, M.; Kwon, Y. J.; Miyazava, M.; Ogura, K. *J. Chem. Soc., Chem. Commun.* **1994**, 1977.
(30) Roesky, H. W.; Andruh, M. *Coord. Chem. Rev.* **2003**, *91*, 236.
(31) Barandika, M. G.; Hernández-Pino, M. L.; Urtiaga, M. K.; Cortés, R.; Lezama, L.; Arriortua, M. I.; Rojo, T. *J. Chem. Soc., Dalton Trans.* **2000**, 1469.

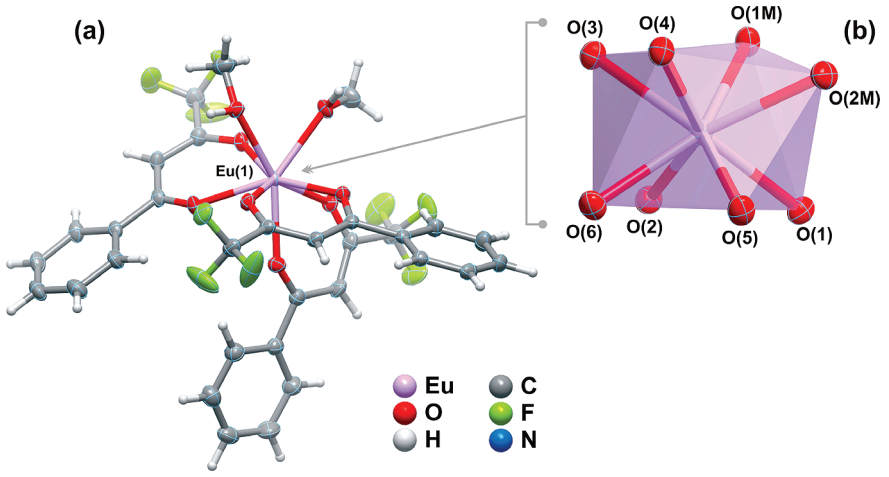

Figure 1. (a) Schematic representation of the $[Eu(btfa)_3(MeOH)_2]$ complex with all non-hydrogen atoms represented as thermal ellipsoids drawn at the 50% probability level, and hydrogen atoms as small spheres with arbitrary radii. For simplicity, only the most probable crystallographic location for the disordered terminal $-CF_3$ group is shown. (b) Polyhedral representation of the distorted square antiprismatic $\{EuO_8\}$ coordination environment for Eu^{3+}, showing the labeling scheme for all atoms composing the first coordination sphere. For selected bond lengths and angles see Table S1 in Supporting Information.

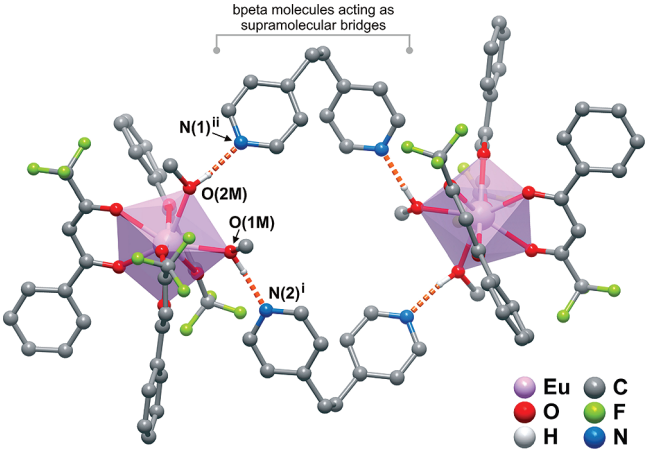

Figure 2. Hydrogen bonding interactions (orange dashed lines) associated with the coordinated MeOH molecules which connect two adjacent $[Eu(btfa)_3(MeOH)_2]$ complexes (via the uncoordinated bpeta molecules) to form a supramolecular dimer. Hydrogen atoms bound to carbon have been omitted for clarity purposes. Hydrogen bonding geometric details: O(1M)−H(1M)···N(2)^{i}, d(D···A) = 2.634(2) Å, ∠(DHA) = 169(3)°; O(2M)−H(2M)···N(1)^{ii}, d(D···A) = 2.723(3) Å, ∠(DHA) = 167(3)°. Symmetry transformations used to generate equivalent atoms: (i) $-1 + x, y, z$; (ii) $-x, 1 - y, 1 - z$.

Scheme 1. Picture of the Incorporation of the $[Eu(btfa)_3(MetOH)_2]\cdot$bpeta Complex into the d-U(600) Host

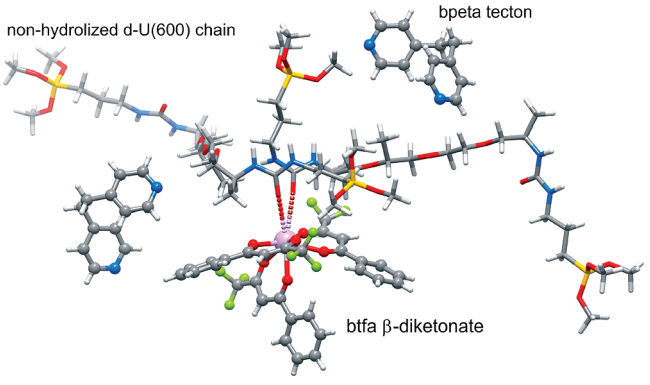

emphasizing the fact that the hybrid network acts a ligand itself. The coordinating ability of the functional groups of the host hybrid is clearly strong enough to induce dramatic changes on the Eu^{3+} local coordination, promoting a strong Eu^{3+}/O=C(hybrid) interaction that is crucial for the improvement the host-to-Eu^{3+} energy transfer. However, this effect has been already observed in analogous Eu^{3+}-containing hybrids.[10,13,14,28,32] Therefore the novelty and significance of the ligands-assisted rational design proposed in this work, which results in an unprecedented emission quantum yield, is determined by the synergy between the btfa and bpeta ligands and the hybrid's emitting centers. As the bpeta chromophore is located in the neighborhood of the hybrid's emitting centers and the btfa ligands, it creates additional and efficient bpeta-to-hybrid and bpeta-to-btfa transfer channels that optimize the overall metal sensitization process contributing therefore for the large emission quantum yields observed. Moreover, this is the first example in which the embedding of a nonaquo Eu^{3+}-β-diketonate complex results in an increase of the emission quantum yield (from 0.58 to 0.60). In all the other cases, severe steric hindrance between the polymer chains of the host structure and bulky highly chelating ligands, such as phen (where phen is 1,10-phenanthroline) in $Eu(btfa)_3phen$[33] and bpy in $Eu(nta)_3bpy$,[13] promoted the expulsion of the latter ligands from the first coordination shell and to their replacement by quenching water molecules with the subsequent reduction of the emission quantum yield (and the $^5D_0$ quantum efficiency). Therefore, a suitable choice of light harvesting ligands with high absorption cross sections, smartly designed to optimize the overall Ln^{3+} sensitization mechanism, definitely endorses the

(32) Molina, C.; Dahmouche, K.; Messaddeq, Y.; Ribeiro, S. J. L.; Silva, M. A. P.; de Zea Bermudez, V.; Carlos, L. D. *J. Lumin.* **2003**, *104*, 93.

(33) Fernandes, M.; Nobre, S. S.; Gonçalves, M. C.; Charas, A.; Morgado, J.; Ferreira, R. A. S.; Carlos, L. D.; de Zea Bermudez, V. *J. Mater. Chem.* **2009**, *19*, 733.

architecture of nanohybrids with better emission conversion performances and higher absolute quantum yields.

Experimental Section

Synthesis of $[Eu(btfa)_3(MeOH)_2]\cdot$bpeta and $[Gd(btfa)_3(MeOH)_2]\cdot$bpeta, Complex 1 and Complex 2: The chemicals $EuCl_3\cdot 6H_2O$ and $GdCl_3\cdot 6H_2O$ (Aldrich), 4,4,4-trifluoro-l-phenyl-1,3-butanedione (Hbtfa, Aldrich), 1,2-bis(4-pyridyl)ethane (bpeta, Aldrich), ethanol (EtOH, Merck), methanol (MeOH, Merck), and sodium hydroxide (NaOH, Merck) were used as received; 0.1 mmol of $LnCl_3\cdot 6H_2O$ (Ln = Eu and Gd) and 0.3 mmol of Hbtfa were dissolved in 1 mL of MeOH. The pH of the solution was adjusted to 6.5 with a methanolic solution of NaOH. Then 0.1 mmol of bpeta was added to this solution. The resulting mixture was stirred for 24 h at room temperature. The solvent was slowly evaporated at room temperature during 48 h. The compound formed was washed with water and recrystallized in MeOH.

*Complex **1**:* Anal. Calcd (%) for $C_{44}H_{38}EuF_9N_2O_8$ C 50.49, H 3.63, N 2.68; Found C 50.41, H 3.54, N 2.63; selected FT-IR data (cm^{-1}) 3443, 3048, 1617, 1578, 1489, 1436, 1064, 631.

*Complex **2**:* Anal. Calcd (%) for $C_{44}H_{38}GdF_9N_2O_8$ C 50.25, H 3.62, N 2.66; Found C 50.32, H 3.68, N 2.61; selected FT-IR data (cm^{-1}) 3450, 3081, 1611, 1577, 1491, 1441, 1061, 632.

Synthesis of d-U(600)-1 and d-U(600)-2: The chemicals Jeffamine ED-600 (Fluka), tetrahydrofurane (THF, Riedel-de Haën), and 3-isocyanatepropyltriethoxysilane (ICPTES, Fluka) were used as received. The synthesis of the di-ureasils has already been described in detail elsewhere.[27] The first step of their preparation involved the reaction in THF of the isocyanate group of the alkoxysilane precursor ICPTES with the terminal amine groups of the double functional diamine Jeffamine ED-600 to form a urea cross-linked organic−inorganic hybrid precursor, so-called ureapropyltriethoxysilane (d-UPTES(600)). In the second step, an appropriate amount (0.0191 mmol) of complexes **1** and **2** was incorporated as ethanolic solutions. The Eu^{3+} complex content versus the total hybrid's mass is 1.1%, corresponding to ether-type oxygen atoms of PEO chains per Eu^{3+} atom ratio equal to *ca.* 780.

Step 1. A volume of Jeffamine ED-600 (1.0 mL, 1.75 mmol) was dissolved in 5.0 mL of dried THF in a flask in a fume cupboard. A volume of ICPTES (0.91 mL, 3.5 mmol) was then added to this solution under stirring. The molar ratio of Jeffamine ED-600 to ICPTES was 1:2. The flask was sealed, and the solution was stirred at room temperature for 24 h.

Step 2. A typical synthetic procedure is presented for d-U(600)-**1** and d-U(600)-**2** prepared with 0.5 M HCl: A mass of 20 mg of complex (Eu^{3+} and Gd^{3+}) was dissolved in CH_3CH_2OH (0.82 mL, 14.04 mmol), and a volume of HCl 0.5 M (0.04 mL) and H_2O (0.051 mL) was added to this solution. The molar ratio of ICPTES:CH_3CH_2OH was 1:4. Finally, the mixed solution was added to the precursor under stirring at room temperature. The samples were obtained as transparent monoliths. The gelation time was 20 min at room temperature. The samples were aged for seven days at 45 °C.

Fourier Transform Infrared Spectroscopy (FT-IR). Mid-infrared spectra were recorded at room temperature using a MATTSON 7000 FTIR Spectrometer. The spectra were collected over the range 4000−400 cm^{-1} by averaging 64 scans at a maximum resolution of 4 cm^{-1}. The compounds were finely ground (about 2 mg), mixed with approximately 175 mg of dried KBr (Merck, spectroscopic grade), and pressed into pellets. Consecutive spectra were recorded until reproducible results were obtained. To evaluate complex band envelopes and to identify underlying component bands of the spectra, the iterative least-squares curve-fitting procedure in PeakFit software was used extensively throughout this study. The best fit of the experimental data was sought by varying the frequency, bandwidth, and intensity of the bands and by employing Voigt band shapes (a mixture of Lorentzian and Gaussian contributions). A linear baseline correction with a tolerance of 0.2% was employed. The standard errors of the curve-fitting procedure were less than 0.003.

Elemental Analysis. The lanthanide content was obtained by ICP-OES (Inductively Coupled Plasma Optical Emission Spectroscopy) analysis on an Horiba-Jobin Yvon model Activa-M at the Central Analytical Laboratory of the University of Aveiro. Elemental analyses for C, H and N were performed with a CHNS-932 elemental analyser with standard combustion conditions and handling of the samples at air.

The thermal characteristics of the samples were investigated using a Setaram DSC 131 differential scanning calorimeter. A disk section with a mass of approximately 20−30 mg was placed in a 40 mL aluminum can and stored in a desiccator over phosphorus pentoxide (P_2O_5) for 1 week at room temperature under vacuum. After this drying treatment, the cans were hermetically sealed and the thermograms were recorded. Each sample was quenched from room temperature to −100 °C and then heated up to 100 at 10 °C min^{-1}. The purge gas used was high-purity nitrogen supplied at a constant 35 mL min^{-1} flow rate. The xerogel sample was also studied by means of thermogravimetric analysis (TGA) using a TA Instruments Q50 thermobalance. In the TGA experiments, the samples were analyzed from room temperature up to 900 °C at a heating rate of 10 °C min^{-1}. The purging gas employed was dried nitrogen (40 mL min^{-1}).

UV−visible Absorption. The UV−visible absorption spectrum was recorded on a JASCO V−560 instrument by using a 10^{-5} mol dm^{-3} methanol solution of the complex **1** and bpeta ligand.

Photoluminescence. The luminescence spectra were recorded with a modular double grating excitation spectrofluorimeter with a TRIAX 320 emission monochromator (Fluorolog-3, Jobin Yvon−Spex) coupled to a R928 Hamamatsu photomultiplier, using the front face

(34) Carlos, L. D.; de Zea Bermudez, V.; Ferreira, R. A. S.; Marques, L.; Assunção, M. *Chem. Mater.* **1999**, *11*, 581.

acquisition mode. The excitation source was a 450W Xe arc lamp. The emission spectra were corrected for detection and optical spectral response of the spectrofluorimeter and the excitation spectra were corrected for the spectral distribution of the lamp intensity using a photodiode reference detector. The lifetime measurements were acquired with the setup described for the luminescence spectra using a pulsed Xe−Hg lamp (6 μs pulse at half width and 20−30 μs tail).

Photodegradation. The photodegradation in the UV-A was investigated by monitoring the $^5D_0 \rightarrow {}^7F_{0-4}$ integrated emission intensity using a Jobin Yvon-Spex spectrometer (HR 460) coupled to a R928 Hamamatsu photomultiplier, under continuous excitation of a Xe arc lamp (150 mW) coupled to a Jobin Yvon monochromator (TRIAX 180). The spectra were corrected for the response of the detector.

Emission Quantum Yield. The emission quantum yield for the complex **1** and d-U(600)-**1** were measured using a quantum yield measurement system C9920-02 from Hamamatsu with a 150W Xe lamp coupled to a monochromator for wavelength discrimination, an integrating sphere as sample chamber and a multichannel analyzer for signal detection. The errors in the quantum yields values associated with this technique were estimated within 10%.

Single-Crystal X-ray Diffraction Studies. Crystalline material of $[Eu(btfa)_3(MeOH)_2]\cdot$bpeta was manually selected from the crystallization vial with the help of a Stemi 2000 stereomicroscope (equipped with Carl Zeiss lenses) and immersed in highly viscous FOMBLIN Y perfluoropolyether vacuum oil (LVAC 140/13) purchased from Sigma-Aldrich.[35] A suitable single-crystal was mounted on a Hampton Research CryoLoop, and data were collected at 100(2) K on a Bruker X8 Kappa APEX II charge-coupled device (CCD) area-detector diffractometer (Mo Kα graphite-monochromated radiation, λ = 0.71073 Å) controlled by the APEX2 software package[36] and equipped with an Oxford Cryosystems Series 700 cryostream monitored remotely using the software interface Cryopad.[37] Images were processed using the software package SAINT+,[38] and data were corrected for absorption by the multi-scan semi-empirical method implemented in SADABS.[39] The structure was solved using the Patterson synthesis algorithm implemented in SHELXS-97,[40,41] which allowed the immediate location of the europium metallic center. All remaining non-hydrogen atoms were located from difference Fourier maps calculated from successive full-matrix least-squares refinement cycles on F^2 using SHELXL-97.[41,42] All non-hydrogen atoms were successfully refined using anisotropic displacement parameters.

One terminal $-CF_3$ group was found to be severely affected by thermal disorder. This group was modeled into the final structural model over two distinct crystallographic positions with fixed rates of occupancy of 1/3 and 2/3, respectively (approximate values found after unrestrained structural refinement for the site occupancies). To ensure a chemically reasonable geometry for this disordered chemical moiety the C−F and F···F distances were further restrained to common, but refinable, values which ultimately converged to 1.311(1) and 2.098(1) Å, respectively.

Hydrogen atoms bound to carbon were located at their idealized positions using appropriate HFIX instructions in SHELXL (*43* for the aromatic and the conjugated carbon atom belonging to the β-diketonate groups, and *23* or *137* for the $-CH_2-$ moieties or terminal methyl groups, respectively) and included in subsequent refinement cycles in riding-motion approximation with isotropic thermal displacements parameters (U_{iso}) fixed at 1.2 (for the two former family of hydrogen atoms) or 1.5 (for the methyl moieties) times U_{eq} of the carbon atom to which they are attached. Hydrogen atoms associated with the coordinated −OH groups of the methanol residues were markedly visible from difference Fourier maps and were included in the final structural model having the O−H distances restrained to 0.95(1) Å. These hydrogen atoms were further allowed to ride on their parent oxygen atoms with $U_{iso} = 1.5 \times U_{eq}(O)$.

The last difference Fourier map synthesis showed the highest peak (1.751 e Å^{-3}) and deepest hole (−0.837 e Å^{-3}) located at 0.83 and 0.42 Å from H(2M3) and H(37B), respectively.

Powder X-ray diffraction data (PXRD) of complexes **1** and **2** were collected at ambient temperature (*ca.* 298 K) on a X'Pert MPD Philips diffractometer (Cu Kα X-radiation, λ = 1.54060 Å), equipped with a X'Celerator detector, a curved graphite-monochromated radiation and a flat-plate sample holder, in a Bragg−Brentano para-focusing optics configuration (40 kV, 50 mA). Intensity data were collected in continuous step scanning mode (0.04°, 5s per step interval) in the range of $3 \leq 2\theta^\circ \leq 50$.

Results and Discussion

X-ray Crystal Structure. The reaction between Hbtfa and bpeta with Eu^{3+} cations included as a chloride salt in MeOH led to the isolation of complex **1** (see Experimental Section) whose structure has been unveiled from single−crystal X−ray diffraction (in combination with CHN elemental analysis), and ultimately formulated as $[Eu(btfa)_3(MetOH)_2]\cdot$bpeta. The complex crystallizes in the centrosymmetric triclinic $P\bar{1}$ space group (Table 1), with the asymmetric unit comprising a whole neutral $[Eu(btfa)_3(MeOH)_2]$ complex which is further engaged

(35) Kottke, T.; Stalke, D. *J. Appl. Crystallogr.* **1993**, *26*, 615.
(36) APEX2, Data Collection Software, version 2.1-RC13; Bruker AXS: Delft, The Netherlands, **2006**.
(37) Cryopad, Remote Monitoring and Control, version 1.451; Oxford Cryosystems: Oxford, U.K., **2006**.
(38) SAINT+, Data Integration Engine, version 7.23a; Bruker AXS: Madison, WI, **1997−2005**.
(39) Sheldrick, G. M. SADABS, version.2.01; Bruker AXS: Madison, WI, **1998**.
(40) Sheldrick, G. M. SHELXS-97, Program for Crystal Structure Solution; University of Göttingen: Göttingen, Germany, **1997**.
(41) Sheldrick, G. M. *Acta Crystallogr. A* **2008**, *64*, 112.
(42) Sheldrick, G. M. SHELXL-97, Program for Crystal Structure Refinement; University of Göttingen: Göttingen, Germany, **1997**.

Table 1. Crystal and Structure Refinement Data for $[Eu(btfa)_3(MeOH)_2]\cdot bpeta$

formula	$C_{44}H_{38}EuF_9N_2O_8$
fw	1045.72
cryst syst	Triclinic
space group	$P\bar{1}$
a/Å	10.6964(2)
b/Å	11.0670(3)
c/Å	19.2250(4)
α/deg	83.6290(1)
β/deg	77.3810(1)
γ/deg	79.5840(1)
vol/Å^3	2178.17(9)
Z	2
D_c/g cm^{-3}	1.594
μ(Mo Kα)/mm^{-1}	1.533
cryst size/mm	0.30 × 0.22 × 0.15
cryst type	Colorless blocks
θ range	3.64 to 30.03
index ranges	$-15 \le h \le 14$ $-15 \le k \le 15$ $-27 \le l \le 27$
reflns collected	82681
independent reflns	12664 (R_{int} = 0.0329)
completeness to θ = 30.03°	99.4%
final R indices [$I > 2\sigma(I)$][a,b]	$R1$ = 0.0295 w$R2$ = 0.0651
final R indices (all data)[a,b]	$R1$ = 0.0355 w$R2$ = 0.0671
weighting scheme[c]	m = 0.0255 n = 2.1466
largest diff. peak and hole	1.751 and −0.837 eÅ^{-3}

[a] $R1 = \Sigma||F_o| - |F_c||/\Sigma|F_o|$. [b] $wR2 = \{\Sigma[w(F_o^2 - F_c^2)^2]/\Sigma[w(F_o^2)^2]\}^{1/2}$. [c] $w = 1/[\sigma^2(F_o^2) + (mP)^2 + nP]$, where $P = (F_o^2 + 2F_c^2)/3$.

in strong and highly directional hydrogen bonds with an uncoordinated, and also crystallographically independent, bpeta residue (see details below). We have recently described a related complex, [Ln(btfa)$_3$(4,4′-bpy)(EtOH)] (Ln = Eu and Gd), which differs from complex **1** in the type of interaction established between the bipyridinic organic molecule and the lanthanide center: direct in the former complex and indirect in the present case.[10]

A search in the literature and in the Cambridge Structural Database (CSD, version 5.30 with one update, November 2008)[43,44] reveals the existence of a considerable number of discrete structures in which lanthanide centers are coordinated to anionic β-diketonate residues. However, only a handful of them contain either MeOH[45] or EtOH[10,46−48] moieties coordinated to the lanthanide centers and composing the first coordination sphere. Moreover, the [Eu(btfa)$_3$(MeOH)$_2$] complex constitutes, to the best of our knowledge, one of the few examples of complexes fully characterized in the solid state having two identical solvent molecules (other than water) directly bound to the lanthanide center: on the one hand, only complexes of this kind with DMF and pyridine coordinated to Eu^{3+} are known;[9] on the other, the structures by Teotonio et al.[47] and De Silva et al.,[48] which correspond to a more common family of complexes, have indeed a combination of EtOH and water in the first coordination sphere of Eu^{3+}.

The neutral [Eu(btfa)$_3$(MeOH)$_2$] complex is composed of a single crystallographically independent lanthanide center coordinated to eight oxygen atoms from three btfa anionic residues plus two MeOH moieties (Figure 1a), overall describing an eight-coordination sphere, {EuO$_8$}, which strongly resembles a distorted square antiprism (Figure 1b): on the one hand, the Eu−O bond distances range from 2.3516(14) to 2.4368(15) Å, with the two longer connections being those established with the coordinated MeOH moieties; on the other, the range of internal O−Eu−O angles for each base of the square antiprism are markedly distinct, ranging from 71.15(5)° to 76.83(5)° for the O(3) → O(4) → O(2M) → O(1M) base, and from 70.56(5)° to 78.96(5)° for the O(6) → O(5) → O(1) → O(2) base (Figure 1b and Table S1 of Supporting Information).

Each crystallographically independent anionic btfa residue appears in complex **1** *O,O*-chelated to the Eu^{3+} center via the ketone functional groups, leading to the formation of six−membered chelate rings as depicted in Figure 1a. The average bite angle for these moieties is of ca. 70.9° (Table S1 of Supporting Information).), which is in good agreement with those typically found in β-diketonate complexes as revealed by a systematic search in the CSD. The spatial distribution of these chelating ligands around the Eu^{3+} coordination polyhedron is markedly distinct from that reported by us for the [Ln(btfa)3(4,4′-bpy)(EtOH)] complexes (Ln = Eu and Gd):[10] while in the latter compounds the three crystallographically independent btfa moieties are orientated in the same direction to minimize steric repulsion with the coordinated 4,4′-bpy, in complex **1** the btfa composing the O(3) → O(4) → O(2M) → O(1M) basal plane is flipped with respect to the other two btfa in the complex. This seems to occur because of a combination of two distinct structural features: first, the absence of other bulky coordinating ligands promotes a different spatial distribution of btfa residues in order to further minimize the overall steric hindrance; second, the N(2)-containing aromatic ring of the uncoordinated bpeta residue is simultaneously engaged in an offset $\pi-\pi$ contact with one coordinated btfa residue (intercentroid distance of about 3.8 Å), and also in a weak C−H···π contact [d(C···π) = 3.6 Å and $\angle$(CHπ) = 145°, where π stands for the centroid of the aromatic ring] with an adjacent btfa residue (interactions not shown). Indeed, the latter cooperative effect can only occur due to the flipped orientation of one btfa ligand. It is worth mentioning that the second pyridinic aromatic ring of the uncoordinated bpeta residue [that containing N(1)] is also engaged in a second offset $\pi-\pi$ contact with a symmetry-identical ring (not shown).

The structurally most significant supramolecular contacts present in complex **1** concern the strong [d(D···A) of 2.634(2) and 2.723(3) Å] and highly directional

(43) Allen, F. H. *Acta Crystallogr. B* **2002**, *58*, 380.
(44) Allen, F. H.; Motherwell, W. D. S. *Acta Crystallogr. B* **2002**, *58*, 407.
(45) Seward, C.; Wang, S. *Can. J. Chem.* **2001**, *79*, 1187.
(46) De Silva, C. R.; Maeyer, J. R.; Wang, R. Y.; Nichol, G. S.; Zheng, Z. *Inorg. Chim. Acta* **2007**, *360*, 3543.
(47) Teotonio, E. E. S.; Brito, H. F.; Viertler, H.; Faustino, W. M.; Malta, O. L.; de Sá, G. F.; Felinto, M.; Santos, R. H. A.; Cremona, M. *Polyhedron* **2006**, *25*, 3488.
(48) De Silva, C. R.; Wang, R. Y.; Zheng, Z. P. *Polyhedron* **2006**, *25*, 3449.

[∠(DHA) greater than 167°] hydrogen bonds connecting the uncoordinated bpeta residues to the coordinated MeOH molecules, which donate the hydrogen atoms from the hydroxyl groups to establish the linkages (Figure 2). Indeed, as depicted in Figure 2, adjacent $[Eu(btfa)_3(MeOH)_2]$ complexes are interconnected via supramolecular bridges formed by two bpeta molecules, leading to the formation of supramolecular dimers. Even though hydrogen bonding interactions of uncoordinated species with solvent molecules composing the first coordination sphere have already been reported by us,[10] De Silva et al.,[46,48] and Seward et al.,[45] this type of arrangement is, to the best of our knowledge, completely unprecedented among this type of lanthanide-based complexes. Because of the strong nature and cooperative effect of these hydrogen bonding interactions it is feasible to assume that this arrangement favors the inclusion of the complexes in the organic−inorganic hybrid matrix used in this research work. Indeed, upon inclusion, the registered hydrogen bonds may facilitate the removal of the solvent molecules from the first coordination sphere, thus allowing the coordinating functional groups from the hybrid polymer to interact with the lanthanide center with a minimal variation of the coordination geometry. Moreover, these strong interactions may lead to a statistical variation of the $Eu-O_{MeOH}$ bonds throughout the entire crystal volume (which ultimately results in the average values reported in Table 1), thus possibly explaining the two lifetimes observed in the photoluminescence studies. Indeed, a search in the latest version of the CSD reveals 15 structures having Eu^{3+} coordinated to MeOH for which the Eu−O bond distances can vary from 2.36 to 2.60 Å.

On the basis of powder X-ray diffraction studies (Figure S1 of Supporting Information), we can infer that the crystalline structures of complexes **1** and **2** are indeed similar and that the crystal details described in the previous paragraphs are representative of the bulk materials.

DSC and TGA analysis. The DSC curves of complex **1** and the corresponding d-U(600)-based sample are shown in Figure 3a. These thermal data indicate that the hybrid sample is entirely amorphous, the broad endothermic peak centered around 85 °C (onset at *ca.* 60 °C) being ascribed to the evaporation of a minor amount of adsorbed water or synthesis solvents (THF and/or ethanol). The DSC curve of the complex exhibits an ill-resolved peak centered at about 124 (onset at ca. 65 °C) with a shoulder around 134 °C. Both thermal events are tentatively assigned to the release of the two methanol molecules present in the first coordination sphere of the lanthanide ion and thus strongly bonded to the Eu^{3+} ion.

The TGA curves of Figure 3b demonstrate that in a nonoxidizing atmosphere the thermal stability of the hybrid is significantly higher than that of the complex for which decomposition is detected already around 65 °C. The latter conclusion is thus in perfect agreement with the DSC data. The degradation of the hybrid sample starts at temperatures higher than approximately 200 °C. We note that at 900 °C, only 45% of this material has

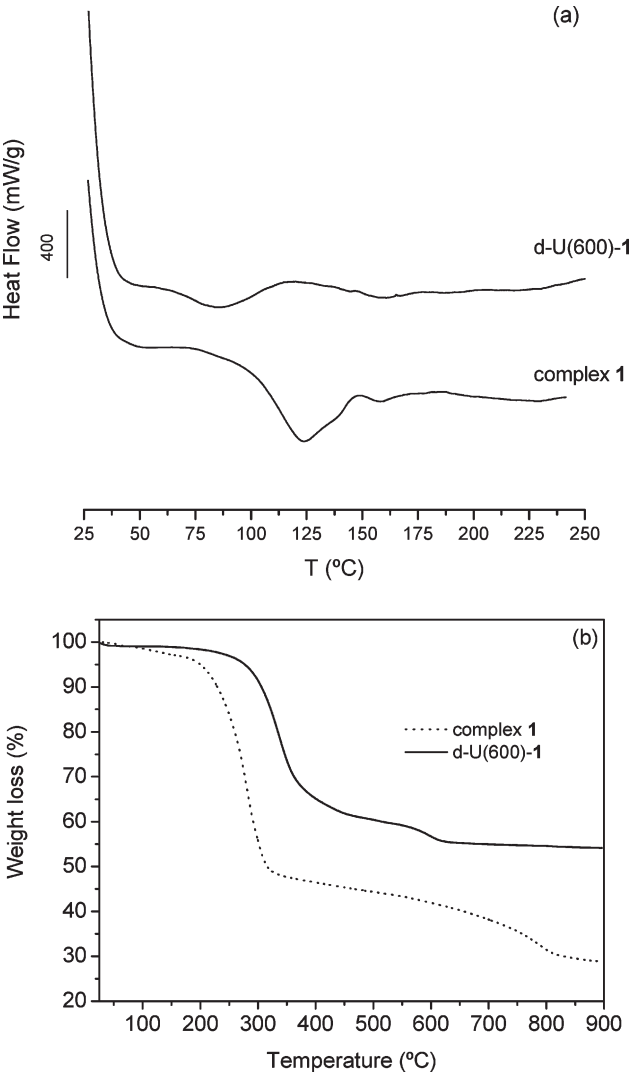

Figure 3. DSC (a) and TGA (b) curves of the complex **1** and d-U(600)-**1**.

decomposed. In contrast, less than 30% of the initial mass of the complex remain at the same temperature.

Fourier Transform Infrared Spectroscopy (FT-IR). Seeking further confirmation of the Eu^{3+}-local coordination in the hybrid host through the oxygen atoms of the C=O groups of the urea cross−linkages, we decided to employ classical curve−fitting procedures in the 1800−1600 cm^{-1} interval to inspect the "Amide I" region of the FT-IR spectrum of d-U(600)-**1** and compare it with that of d-U(600).[27,49,50] In this frequency region, the nondoped hybrid matrix produces three individual components centered at about at ~1720, 1686, and 1662 cm^{-1} (Figure 4a), assigned to the absorption of hydrogen-bonded C=O groups of disordered POE/urea aggregates of increasing strength (**D3**, **D2**, and **D1**, respectively).[27,49,50] A prominent band also appears around 1640 cm^{-1} because of the absorption of C=O groups included in significantly more ordered hydrogen-bonded

(49) Nunes, S. C.; de Zea Bermudez, V.; Ostrovskii, D.; Carlos, L. D. *J. Mol. Struct.* **2004**, *39*, 702.
(50) Fu, L.; Ferreira, R. A. S.; Fernandes, M.; Nunes, S. C.; de Zea Bermudez, V.; Hungerford, G.; Rocha, J.; Carlos, L. D. *Opt. Mater.* **2008**, *30*, 1058.

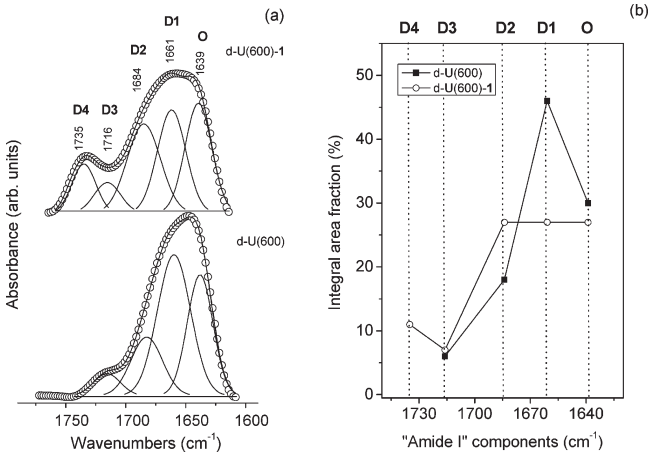

Figure 4. Curve-fitting results of the FT-IR Amide I region of d-U(600) and d-U(600)-**1** (a). The frequencies indicated represent the average value of the frequencies observed in both spectra. Integral area fraction of the resolved components of the Amide I bands of d-U(600) and d-U(600)-**1** (b).

urea−urea aggregates (**O**).[27,49,50] The results of the curve-fitting performed in the 'Amide I' band of d-U(600) and d-U(600)-**1** (Figure 4a) and the plot that represents the integral area fraction of the resolved components (Figure 4b) clearly demonstrate that the inclusion of the $[Eu(btfa)_3(MeOH)_2]$bpeta complex into d-U(600) has major consequences in the hydrogen-bonded array of this hybrid matrix: (1) The intensity maximum of the 'Amide I' profile shifts to higher frequencies (from 1644 to 1654 cm^{-1}), meaning that the hydrogen bonds become globally weaker. (2) While the intensity of the 1640 cm^{-1} component is slightly reduced, that of the 1662 cm^{-1} component is subject to an abrupt drop (*ca.* 20%). These findings are indicative of the disruption of a minor fraction of the urea−urea aggregates **O** and of the destruction of a significant proportion of the strongest POE/urea aggregates **D1**, respectively. (3) In parallel, the intensity of the 1686 cm^{-1} component is subject to a marked increase (10%), suggesting the formation of more POE/urea aggregates **D2**. (4) In the FT-IR spectrum of d-U(600)-**1**, the new band centered at 1735 cm^{-1}, formed at the expense of the breakdown of aggregates **O** and, especially, **D1**, is associated with the occurrence of new POE/urea hydrogen-bonded aggregates more disordered than aggregates **D3**. We note that it does not correspond to any of the C=O environments reported for the non-doped di-ureasils.[27,49,50] (5) In a manner similar to the situation found in the case of d-U(600),[27,49,50] the 1750 cm^{-1} band, attributed to "free" C=O groups devoid of any hydrogen bonding interactions, is missing in the FT-IR spectrum of d-U(600)-**1** (Figure 4a). Typically, in di-ureasils, the coordination of lanthanide ions (introduced as a complex) to the C=O oxygen atoms of the urea cross-linkages of the hybrid matrix is easily monitored in the Amide I region through the detection of a new event around 1620 cm^{-1}.[13,14] Although this Eu^{3+} coordination-sensitive feature is not seen in Figure 4a, it is likely that the concentration of Eu^{3+} is too low to yield a detectable band by FT-IR. Moreover, the possibility that a new band is masked by the broad component centered at about 1639 cm^{-1} cannot be discarded either. Considering the magnitude of the perturbation of the complex on the hydrogen-bonded array of d-U(600), the spectroscopic modifications described above do not result simply from hindrance effects associated with the bulkiness of the ligands, but in particular to the establishment of Eu^{3+}/O=C (urea) bonds.

To further determine if the entrance of the C=O groups of the urea cross-linkages of d-U(600) in the first coordination sphere of the Eu^{3+} ions in the complex had any consequences of the conformational state of the POE chains of the host d-U(600) di-ureasil matrix, we inspected two regions of the FT-IR spectra of d-U(600)-**1** that are known to be sensitive to modifications of the POE backbone conformations: the rCH_2 region (980−900 cm^{-1}) and the CH_2 scissoring and CH_3 deformation region (1500−1400 cm^{-1}). In the rCH_2 band envelope of d-U(600)-**1** (Figure S2a of Supporting Information) the most important aspect worth referring is the emergence of a new feature at 937 cm^{-1}, characteristic of crystalline high molecular weight poly(ethylene glycol)dimethyl ether (PEGDME).[51] Between 1500 and 1400 cm^{-1} the spectral band profile of d-U(600)-**1** is deeply modified (Figure S2b of Supporting Information). The most significant change detected in this wavenumber interval is the presence of a new band of medium intensity at 1467 cm^{-1} and several new shoulders. The 1467 cm^{-1} feature is also produced by crystalline PEGDME.[51] These data lead us to conclude that complex addition clearly leads to a reduction of the segmental mobility of the disordered POE chains of d-U(600). Thus the local degree of order of the chains increases, meaning that the population of gauche conformers increases too.

Photoluminescence. Figure 5 displays the low-temperature emission spectra for complex **1** excited at two different excitation wavelengths (462.9 and 465.3 nm). The emission spectra display the typical Eu^{3+} intra−$4f^6$ lines ascribed to the $^5D_0 \rightarrow {}^7F_{0-4}$ transitions. Upon increasing the excitation wavelength from 462.9 to 465.3 nm a red−shift of ca. 5 cm^{-1} for the $^5D_0 \rightarrow {}^7F_0$ transition is observed, which suggests a large distribution of Eu^{3+}-local environments, since this transition occurs between non−degenerated states. The relative intensity of the $^7F_{1,2}$ Stark levels also changes with the change of the excitation wavelength. Furthermore, the $^5D_0 \rightarrow {}^7F_{1-2}$ transitions clearly exhibit 4 and 7 Stark components, respectively. All these observations point out the presence of closely similar Eu^{3+} sites in agreement with a statistical variation of the $Eu-O_{MeOH}$ bonds throughout the entire crystal volume (XRD results). Complex **1** photoluminescence intensity decreases around 38% after 6 h under UV-A (365 nm) irradiation illustrating the photobleaching process typical of β-diketonates chelates.[9,10] This effect of Eu^{3+} luminescence quenching is irreversible and leads to

(51) Matsuura, H.; Miyazawa, T.; Machida, K. *Spectrochim. Acta* **1973**, *29A*, 771.

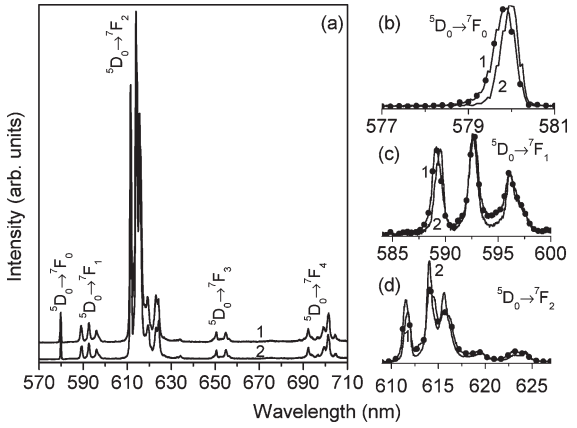

Figure 5. (a) Emission spectra (11 K) of complex **1** excited at (1) 462.9 nm and (2) 465.3 nm. (b), (c), and (d) show a magnification of the $^5D_0 \rightarrow ^7F_{0-2}$ transitions.

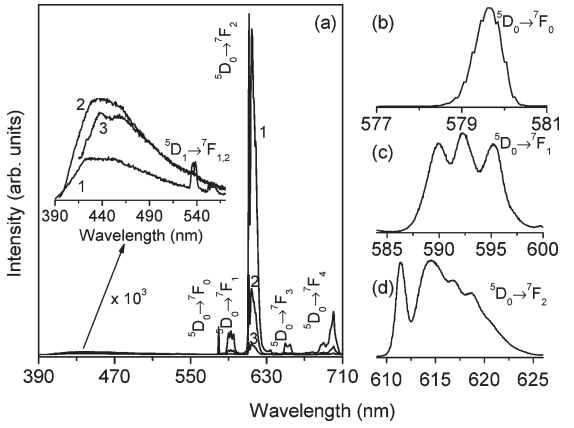

Figure 6. (a) Emission spectra (11 K) of d-U(600)-**1** excited at (1) 370, (2) 380, and (3) 400 nm. (b, c, and d) A magnification of the $^5D_0 \rightarrow ^7F_{0-2}$ excited at 370 nm.

a memory effect that has been used to develop thin film Ln^{3+}-based UV dosimeters.[52] The discussion of the photodegradation mechanism of complex **1** is beyond the scope of the present manuscript and will be addressed in detail in a subsequent publication.

The emission features after the complex incorporation into the di-ureasil host are shown in Figure 6. The emission spectra of the d-U(600)-**1** display the intra-4f^6 lines between the $^5D_{0,1}$ excited states and the $^7F_{0-4}$ levels of the ground state. The observation of emission arising from higher excited levels such as the $^5D_1$, indicates nonefficient nonradiative relaxation to the $^5D_0$ level. The presence of a single line for the nondegenerated $^5D_0 \rightarrow ^7F_0$ transition, the local field splitting of the $F_{1,2}$ levels into 3 and 5 Stark components, respectively, and the high relative intensity of the $^5D_0 \rightarrow ^7F_2$ transition indicate that the Eu^{3+} ions occupy a low-symmetry local group without an inversion center (in agreement with the XRD description). Comparison of the emission features of complex **1** (Figure 5) with those of the hybrid allows to conclude that the energy and the full-width at half-maximum (fwhm) of the $^5D_0 \rightarrow ^7F_{0-4}$ transitions are strongly altered, indicating an effective interaction between the Eu^{3+} ions and the di-ureasil host. To further quantify the differences in the emission features after complex incorporation, the fwhm and the energy of the $^5D_0 \rightarrow ^7F_0$ transition were estimated by deconvoluting the emission spectra at 11 K for complex **1** and d-U(600)-**1**, assuming a single Gaussian function. The energy of the $^5D_0 \rightarrow ^7F_0$ transition for the d-U(600)-**1** (17253.0 ± 0.1 cm^{-1}) is blue-shifted in comparison with the energy estimated for complex **1** (17246.3 ± 0.2 and 17243.2 ± 0.1 cm^{-1}, excited at 462.9 and 465.3 nm, respectively). The estimated values for the fwhm of the $^5D_0 \rightarrow ^7F_0$ transition are 18.5 ± 0.3 and $11.4-13.5 \pm 0.3$ cm^{-1} for d-U(600)-**1** and complex **1**, respectively. The increase of the fwhm in the hybrid emission lines is related with the essentially amorphous local structure of the host that accommodates in slightly different ways the Eu^{3+} first coordination sphere, thus leading also to slight modifications in the phonon density distribution, in straight agreement with the effective interaction between complex **1** and the d-U(600) host.[10]

The emission spectra of the d-U(600)-**1** are also formed of a low-relative-intensity emission band between 390 and 560 nm (inset in Figure 6a), whose maximum emission energy shifts toward the red as excitation wavelength increases. This is the typical behavior ascribed to the hybrid host intrinsic emission, attributed to the convolution of electron−hole recombinations originated in the NH/C=O groups of the urea cross−linkages and within the siliceous nanoclusters.[24−26] The very low relative intensity of this broadband points out the presence of active hybrid-to-ligands and hybrid-to-Eu^{3+} energy transfer channels.[10]

No emission arising from the β-diketonate ligands could be detected, both in complex **1** and d-U(600)-**1**, a finding that may be interpreted as a proof of an efficient ligands-to-Eu^{3+} energy transfer because ligand emission is observed in complex **2** and in d-U(600)-**2** in the temperature range of 11−300 K, as we will show latter. The photoluminescence intensity of d-U(600)-**1** decreases around 17% after 6 h of UV-A irradiation (365 nm), pointing out a significant enhancement of the UV photostability in the hybrid. Similarly to that mentioned for complex **1**, the detailed study of the photodegradation mechanism in d-U(600)-**1** lies beyond the scope of this work and will be detailed in a further paper.

Figure 7 compares the low-temperature excitation spectra of complex **1** and d-U(600)-**1** monitored at the maximum intensity of the $^5D_0 \rightarrow ^7F_2$ transition. The spectrum of complex **1** is composed of a large structured broadband peaking at 370 nm with three shoulders at high-wavelength (370−460 nm) overlapping a series of narrow lines attributed to transitions between the $^7F_0$ levels and the $^5L_6$, and $^5D_{1,2}$ excited states. While the low-wavelength region of the broadband is related to the excited states of the btfa ligands, as the bpeta-related ones appear at higher energies (Figure S3 of Supporting Information); the high-wavelength region is associated with ligand-to-metal charge transfer (LMCT) states, as demonstrated below. The high relative intensity of the

(52) Gameiro, C. G.; Achete, C. A.; Simão, R. A.; da Silva, E. F., Jr.; Santa-Cruz, P. A. *J. Alloys Compd.* **2002**, *344*, 385.

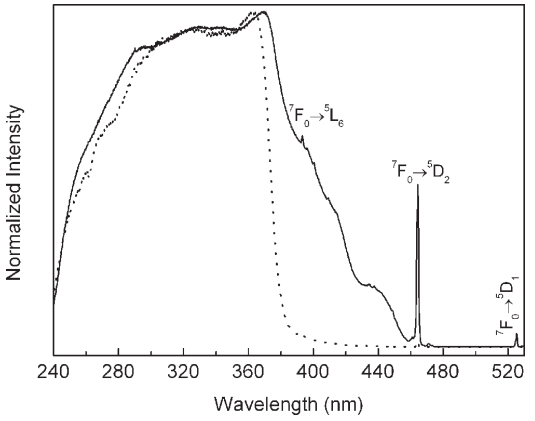

Figure 7. Excitation spectra (11 K) of complex **1** (solid line) and of d-U(600)-**1** (dotted line) monitored at 614 nm.

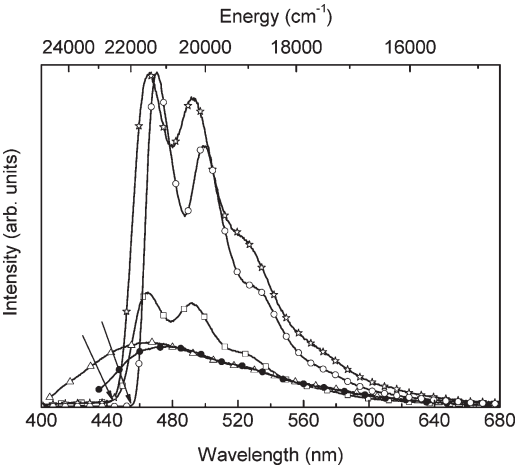

Figure 8. Emission spectra (11 K) of complex **2** excited at 368 nm (○) and (b) d-U(600)-**2** excited at 280 (□), 350 (☆), 390 (△), and 420 nm (●).

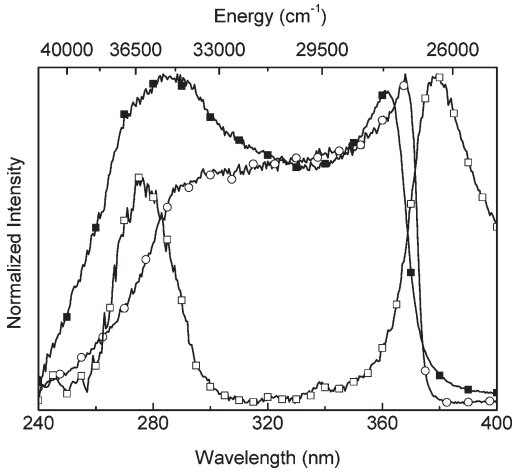

Figure 9. Excitation spectra (11 K) of complex **2** (○) monitored at 470 nm and of d-U(600)-**2**, monitored at 420 (□) and 464 nm (■).

btfa-related band points out a more efficient sensitization process when compared with direct-intra-4f^6 excitation. After complex **1** incorporation, the excitation spectrum for d-U(600)-**1** reveals a large broadband (240−430 nm) and a series of narrow lines with negligible intensity attributed to the $^7F_0 \rightarrow {}^5L_6$, $^5D_{2,1}$ transitions. The decrease in the relative intensity of the intra−4f^6 lines, points out an increase in the Eu^{3+}-sensitization process, when compared with that observed for the isolated complex. The low-wavelength region of the excitation spectrum (240−390 nm) overlaps that measured for complex **1** pointing out the presence of essentially the same btfa-to-Eu^{3+} energy transfer channels. Moreover, comparing this spectrum with that monitored for complex **1**, the narrowing of the d-U(600)-**1** spectrum because of the disappearance of the LMCT components (390−450 nm) can be attributed to an effective interaction between complex **1** and the hybrid. The role of the bpeta states in the population of the Eu^{3+} intra-4f^6 will be detailed next.

To further characterize the ligand-to-Eu^{3+} and the hybrid-to-Eu^{3+} energy-transfer pathways, it was necessary to determine the energy of the ligand states, namely, singlet (S) and triplet (T) levels of the bfta, bpeta, and hybrid host-emitting centers. The energy of these singlet and triplet levels are measured by studying, respectively, the absorption and the luminescence properties of the free bpeta ligand, complex **2** and d-U(600)-**2**. The singlet levels of bpeta ligand and d−U(600)−**1** hybrid were extracted from the corresponding absorption spectrum, considering that the absorption edges correspond to the $0(S_0) \rightarrow 0(S)$ transition (Figures S3 and S4, respectively, of Supporting Information). The triplet excited states were determined from the emission spectra of the Gd^{3+} compounds (arrows in Figure 8) and bpeta ligand (Figure S5 of Supporting Information). This experimental procedure is based on the fact that the Gd^{3+} excited levels have energies much higher than those typical of ligand singlet and triplet states, disabling, therefore, any ligand-to-metal energy transfer process.

Figure 8 shows the emission spectrum of complex **2**, revealing a triplet state energy of 21890 cm^{-1}. The decay curve monitored at such triplet state (470 nm) under excitation at 368 nm displays a single exponential behavior (not shown) with a lifetime value of 1.679 ± 0.005 ms. Such a long-lived emission is in completely agreement with the triplet nature assignment. The excitation spectrum (Figure 9) monitored at 470 nm displays a large broadband (240−390 nm) with a maximum peak position at 368 nm, assigned to the btfa singlet state. When this excitation spectrum is compared with that acquired for complex **1** (Figure 7), the lack of the components within 390−460 nm spectral range in the Gd^{3+} spectra unequivocally indicates that such components can be attributed to LMCT states.

After complex **2** incorporation into the hybrid host, the emission spectra of d-U(600)-**2** (Figure 8) strongly depend on the excitation wavelength. For excitation wavelengths between 300 and 355 nm, the spectra show the typical emission arising from the btfa triplet state at 22437 cm^{-1}, which is a blue shift (*ca.* 250 cm^{-1}) relative to that found for the isolated complex (Figure 8), in agreement with the previously mentioned interaction between the complex and the di-ureasil host. Upon excitation of the d-U(600)-**2** between 385 and 440 nm, the spectra (Figure 8) are composed of a broadband (390−680 nm),

for which the maximum peak position deviates toward the red as the excitation wavelength increases, ascribed to the hybrid host excited states.[24−26] The energy of the hybrid host emitting states is similar to that estimated for the d-U(600) hybrid incorporating [Eu(btfa)$_3$(4,4′-bpy)-(EtOH)].[10]

The excitation spectra for d-U(600)-**2** (Figure 9) were selectively monitored within the btfa triplet state and within the hybrid host excited states at 465 and 420 nm, respectively. The former spectrum shows a broad-band with two main components at 285 and 370 nm ascribed to the bpeta (Figure S3 of Supporting Information) and btfa singlet states, respectively. The excitation spectrum selectively monitored within the hybrid host displays two main components peaking at 285 nm attributed to the bpeta excited states and a broad band within 345 to 405 nm originated between the hybrid's intrinsic emitting levels. The observation of the bpeta excited states (around 285 nm) both in the excitation spectra monitored within the btfa and hybrid host excited states points out the presence of a two-step intermolecular energy transfer between (i) bpeta and btfa, followed by btfa-to-Eu^{3+} energy transfer, and (ii) bpeta and hybrid, followed by hybrid-to-btfa-to-Eu^{3+} and hybrid-to-Eu^{3+} energy transfer. These results show the crucial role of the free bpeta molecule in the population of the Eu^{3+}-emitting levels. Therefore, we may suggest that the most probable channel for the energy transfer process is bpeta → btfa/hybrid → Eu^{3+}(^{5}D$_{1-0}$) → ^{7}F$_{0-6}$, as depicted in the energy diagram in Figure 10.

To quantify the active role of the bpeta excited states in the population of the Eu^{3+} excited levels, the ^{5}D$_0$ emission lifetime values were estimated for complex **1** and d-U(600)-**1** hybrid in the 12−300 K temperature range. For complex **1** and d−U(600)−**1** the emission curves were monitored within the ^{5}D$_0$ → ^{7}F$_2$ transition under the excitation wavelength that maximizes the Eu^{3+} emission intensity (around 370 nm). All the curves are well modeled assuming a single exponential function yielding to lifetime values for complex **1** and d-U(600)-**1** of 0.392 ± 0.002 and 0.658 ± 0.002 ms (11 K) and 0.379 ± 0.001 ms and 0.619 ± 0.002 ms (300 K), respectively. The increase in the ^{5}D$_0$ lifetime values after the complex **1** incorporation into the di-ureasil host is in good agreement with the replacement of the MeOH molecules by oxygen atoms of the C=O groups of the urea cross−linkages.

For d-U(600)-**1**, the ^{5}D$_0$ radiative (A_r) and nonradiative (A_{nr}) transition probabilities and the quantum efficiency (η) [$\eta = A_r/(A_r + A_{nr})$] were estimated on the basis of the emission spectrum and ^{5}D$_0$ lifetime $\tau^{-1} = A_T = A_r + A_{nr}$)[1,7,10,53] The radiative contribution was calculated from the relative intensities of the ^{5}D$_0$ → ^{7}F$_{0-4}$ transitions (the ^{5}D$_0$ → ^{7}F$_{5,6}$ branching ratios were neglected because of their poor relative intensity with respect to that of the remaining ^{5}D$_0$ → ^{7}F$_{0-4}$ lines). The ^{5}D$_0$ → ^{7}F$_1$ transition

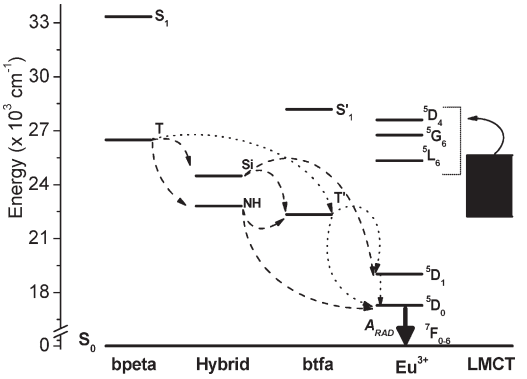

Figure 10. Energy level diagram for the d-U(600)-**1**. The arrows indicate possible energy transfer paths.

does not depend on the local ligand field and thus may be used as a reference for the whole spectrum. An effective refractive index of 1.5 was used leading to $A_{01} \approx 50\ s^{-1}$,[1,7] where A_{01} stands for the Einstein's coefficient of spontaneous emission between the ^{5}D$_0$ and the ^{7}F$_1$ Stark levels. These calculations were not performed for the complex considering the non−homogeneity of the Eu^{3+}−local environments. A q value around 0.63 (Table 2) was found for d-U(600)-**1**. This value is higher than that found for the d-U(600)-based hybrid incorporating the [Eu(btfa)$_3$(4,4′-bpy)(EtOH)] complex (0.53),[10] because of both an increase in the A_r value and a decrease in the A_{nr} one.

The nonradiative transition probability may be rationalized in terms of the number of water molecules (n_w) or number of OH oscillators coordinated to the metal ion trough the empirical formula[54] $n_w = 1.11 \times [A_T - A_r - 0.31]$, where A_T is the reciprocal value of the ^{5}D$_0$ lifetime (Table 2). For the d-U(600)-**1**, the number of OH oscillators coordinated to the Eu^{3+} is 0.31 ± 0.1, confirming the replacement of the two labile MeOH molecules in the Eu^{3+} first-coordination sphere after the hybrid incorporation. The increase of the ^{5}D$_0$ lifetime of the hybrid, relatively to that of the precursor complex, also supports that replacement.

From the room temperature emission spectrum of d-U(600)-**1** (Figure S6 of Supporting Information), we determined the experimental intensity parameters, Ω_2 and Ω_4, (Table 2) by using the ^{5}D$_0$ → ^{7}F$_2$ and ^{5}D$_0$ → ^{7}F$_4$ electronic transitions, respectively, and by expressing the emission intensity $I_j = \hbar\omega_{j0}A_r(J)N(^5D_0)$ in terms of the surface under the emission curve. Here $\hbar\omega_{j0}$ is the transition energy.[1,7,10,53] The magnetic dipole allowed ^{5}D$_0$ → ^{7}F$_1$ transition was taken as the reference.[53] The Ω_6 parameter was not determined, since the ^{5}D$_0$ → ^{7}F$_{5,6}$ transitions are not observed experimentally. The radiative emission rates, $A_r(J)$, are given by

$$A_r(J) = \frac{4e^2\omega^3}{3\hbar c^3}\chi\sum_{\lambda}\Omega_\lambda\langle^7F^J\|U^{(\lambda)}\|^5D^0\rangle^2\frac{1}{2J+1} \qquad (1)$$

(53) de Sá, G. F.; Malta, O. L.; de Mello Donegá, C.; Simas, A. M.; Longo, R. L.; Santa-Cruz, P. A.; da Silva, E. F., Jr. *Coord. Chem. Rev.* **2000**, *196*, 165.

(54) Supkowski, R. M.; Horrocks, W. D. *Inorg. Chim. Acta* **2002**, *340*, 44.

Table 2. $^5D_0$ Lifetime Value (τ), Radiative (A_r) and Nonradiative (A_{nr}) Decay Rates, Quantum Efficiency (η), Emission Quantum Yield (ϕ), and Experimental Intensity Parameters (Ω_2 and Ω_4) for d-U(600)-1[a]

τ [ms]	A_r [ms^{-1}]	A_{nr} [ms^{-1}]	η	ϕ	Ω_2 [10^{-20} cm^2]	Ω_4 [10^{-20} cm^2]
0.619 ± 0.002	1.022	0.593	0.63	0.60	28.3	6.2

[a] The data were obtained at room temperature.

where $\lambda = 2$ and 4, χ is the Lorentz local field correction term that is given by $n(n^2+2)^2/9$, and $\langle {}^7F_J \| U^{(\lambda)} \| {}^5D_0 \rangle^2$ are the squared reduced matrix elements whose values are 0.0032 and 0.0023, for $J = 2$ and 4, respectively.[55] The total radiative emission rate in eq 1 is $\Sigma_J A_r(J)$. The high value of Ω_2 (28.3 10^{-20} cm^2) might be interpreted as a consequence of the hypersensitive behavior of the $^5D_0 \rightarrow {}^7F_2$ transition,[55] suggesting that the dynamic coupling mechanism is quite operative and that the chemical environment is highly polarizable.

Emission Quantum Yield. The room temperature emission quantum yield measured for complex **1** is 0.58 ± 0.06 under excitation at 370 nm. This value is substantially higher than that estimated for the Eu(btfa)$_3 \cdot 2H_2O$ aquocomplex, 0.20.[53,56] Despite the presence of OH oscillators in the Eu^{3+} first coordination sphere of the two complexes (originated from water and MeOH molecules for the aquocomplex and complex **1**, respectively), the higher value found for complex **1** points out the active role in the light harvesting and energy transfer of the bpeta ligand. After complex **1** incorporation into the hybrid, the same value (within the experimental error) was measured for the quantum yield of d-U(600)-**1**, 0.60 ± 0.06, under 307 nm excitation wavelength. We should stress that this value is the highest measured for lanthanide−containing emitting organic−inorganic hybrids and also that this is the first example where no quantum yield degradation was observed after the incorporation of a β-diketonate complex devoid of H_2O ligands into an organic−inorganic host.[1] This is an evidence that despite the possible feeble hybrid−metal ion interaction, potentiated by the strongly chelating of btfa ligand, which in principle disables the replacement of complex ligands by the hybrid matrix coordinating groups,[1] the presence in the complex of appropriate ligands with adequate lability, such as the bpeta ligand, allows to overcome that drawback. After incorporation into the hybrid matrix, the bpeta ligand remains in close proximity to the metal center contributing to the sensitization process and, therefore, to the enhancement of its photoluminescence.

Conclusions

In this work, we discussed the structural and optical features of an organic−inorganic hybrid incorporating the new [Ln(btfa)$_3$(MeOH)$_2$]·bpeta (Ln = Eu and Gd) complexes. These complexes are supramolecular dimers because of the interconnection between two units of [Ln(btfa)$_3$(MeOH)$_2$] (Ln = Eu and Gd) via supramolecular bridges made of hydrogen bonds formed between two bpeta tectons and four MeOH molecules. The Eu^{3+}-based compound further constitutes one of the rare examples of complexes having two identical solvent molecules, other than water, directly bound to the lanthanide center.

The inclusion of complex **1** within the di-ureasil host framework has three major structural effects: (1) The strongly coordinating oxygen atoms of the urea C=O groups of the host hybrid displace the labile MeOH molecules from the lanthanide coordination sphere and replace them. (2) The hydrogen-bonded array of d-U(600) is weakened: a significant proportion of its ordered POE/urea aggregates are broken, more disordered POE/urea aggregates are formed. In parallel new POE/urea aggregates, weaker than those initially present, emerge. (3) The degree of order of the POE chains increases as a result of the increase of the population of gauche conformers.

The calculated number of OH oscillators coordinated to the Eu^{3+} for d-U(600)-**1** (0.31 ± 0.1) confirms the replacement of the two labile MeOH molecules in the Eu^{3+} first-coordination sphere after complex **1** incorporation. Moreover, an increase of approximately 65% in the $^5D_0$ lifetime value after complex **1** addition to the di-ureasil host is in good agreement with the replacement of the MeOH molecules by oxygen atoms of the carbonyl groups of the urea cross-linkages. Moreover, the presence of the bpeta excited states (around 285 nm) in the excitation spectra of the d-U(600)-**2** indicates the presence of a two-step intermolecular bpeta → btfa → Eu^{3+}, bpeta → hybrid → btfa → Eu^{3+}, and hybrid → Eu^{3+} energy transfer. In the light of this approach the bridges formed between the MeOH molecules and the bpeta ligands that initially ensured the formation of the dimer unit were broken, although the bpeta ligand remained located in the Eu^{3+} neighborhood.

The emission quantum yield values for the complex **1** and d-U(600)-**1** are practically identical, 0.58 ± 0.06 and 0.60 ± 0.06, respectively, indicating that the degradation of the complex (and corresponding reduction of the emission quantum yield) does not occur after incorporation into the di-ureasil host. We should point out that the quantum yield value of d-U(600)-**1** is the highest reported so far for lanthanide-containing emitting organic−inorganic hybrids. Furthermore these results support that after complex incorporation the bpeta ligand remains close to the metal center, thus contributing to the sensitization process and, ultimately, to the enhancement of its photoluminescence. The novelty and significance of the ligands-assisted rational design proposed here, resulting

(55) Carnall, W. T.; Crosswhite, H.; Crosswhite, H. M. *Energy Levels, Structure and Transition Probabilities of the Trivalent Lanthanides in LaF3*; Argonne National Laboratory: Argonne, IL, 1997.
(56) Junior, S. A.; de Almeida, F. V.; de Sá, G. F.; Mello Donegá, C. *J. Lumin.* **1997**, *72−74*, 478.

in an unprecedented emission quantum yield, is determined by the synergy between light harvesting cromophores (a classical β-diketonate and a tecton) and the hybrid's emitting centers and opens potential and exciting new perspectives to engineering highly emissive lanthanide-containing organic−inorganic hybrids.

Acknowledgment. This work was supported by Fundação para a Ciência e a Tecnologia (FCT), PTDC FEDER (SFRH/BPD/34365/2006), and EMMI. We are grateful to FCT for the financial support toward the purchase of the single-crystal diffractometer. The authors would like to thank Mariana Fernandes (UTAD, Portugal) for help with the thermal analysis.

Supporting Information Available: Table S1 and Figures S1−S6. This material is available free of charge via the Internet at http://pubs.acs.org.Crystallographic data (excluding structure factors) for the structure reported in this paper have been deposited with the Cambridge Crystallographic Data Centre as supplementary publication No. CCDC-724225. Copies of the data can be obtained free of charge on application to CCDC, 12 Union Road, Cambridge CB2 2EZ, U.K. FAX: (+44) 1223 336033. E-mail: deposit@ccdc.cam.ac.uk.